Closed-Loop Analysis and Control of Cavity Shear Layer Oscillations

Mohamed-Yazid Rizi[1], Luc Pastur[2,3], Mohamed Abbas-turki[1], Yann Fraigneau[1] and Hisham Abou-kandil[2]
[1]SATIE, Ecole Normale Superiéure de Cachan, 94235 Cachan cedex, France.
[2]LIMSI-CNRS, BP 133, 91403 Orsay, France.
[3]Université Paris-Sud 11, 91405 Orsay cedex, France. rizi@satie.ens-cachan.fr

Received date: 19 October 2014; Accepted date: 6 March 2015

ABSTRACT
This paper focuses on the closed-loop control of an incompressible flow past an open cavity. We propose a delayed feedback controller to suppress the self-sustained oscillations of the shear layer. The control law shows robustness to changes in flow conditions. An extension of the Eigensystem Realization Algorithm (ERA) to closed-loop identification, the so-called OCID technique, is used to extract the unstable linear dynamics of the cavity flow. The model-based analysis actually captures the modes against which the steady flow becomes unstable. The identified model is used to design an optimal controller, which shows both efficiency and robustness to stabilize the cavity flow.

1. INTRODUCTION

In numerous applications, self-sustained oscillations are the source of energetic accoustic noise. This is for instance the primary source of noise in high-speed trains, and they also contribute to noise pollution around airports caused by aircraft during landing and takeoff. The flow past an open cavity is well known to give rise to self-sustained oscillations and provides a benchmark configuration for the study of noise reduction strategies.

To fulfill the objectives of control, several strategies have been proposed in open-loop and closed-loop plant designs, over the past twenty years, with actuators that disrupts the flow, either placed at the bottom of the cavity [1], or at the upstream edge where the flow is the most sensitive to velocity changes [2].

This paper focuses on the closed-loop control of an open cavity flow in the incompressible regime. The great challenge is to design a controller able to suppress the self-sustained oscillations of the shear-layer and stabilize the steady base flow. In principle, the flow should be described by a high-dimensional system because it results from the numerical resolution of the Navier-Stokes equations. Unfortunately, these equations are inappropriate for a controller synthesis aimed at working in real-time applications. It is instead required to approximate the system dynamics by a finite-dimensional model. We want to find a technique appropriate for fluid mechanics that produces an accurate reduced-order model able to capture the arising dynamics of the cavity flow, while remaining easy to implement experimentally and achieving real-time performances.

The most widely used method to obtain reduced-order models is POD (Proper Orthogonal Decomposition), combined with Galerkin projection [3]. The resulting POD modes are considered to be the most controllable modes, but their observability is not considered in the construction of a reduced order model, because POD maximizes the average energy of the data in the projection subspace.

In the problem of model reduction to a desired size, controllability and observability are equivalently important because the quality of a reduced model to reproduce the behavior of the original system strongly depends on them. To take into account these two concepts, [4] proposed the so-called *balanced* POD (BPOD) method, which is an extension of balanced truncation for large systems.

In the case of a fluid flow past an open cavity beyond a critical Reynolds number, the steady base flow becomes globally unstable and the dynamics eventually saturate to a limit cycle, due to non-linearities. The study in [5] splits the complete dynamics into two subspaces, one catching the unstable dynamics, spanned by the global modes with positive growth-rate, the other subspace describing the stable dynamics, whose dimension is eventually large. The reduction of the stable subspace dimension is crucial when dealing with the controller synthesis. Authors in [5] showed that models based on BPOD Petrov-Galerkin projection outperform models based on POD for capturing the input-output behavior. Unfortunately, BPOD cannot be applied to experiments since it requires the adjoint state to be determined, which can only be done from numerical simulations [6].

Recently, [7] established an equivalence between BPOD and ERA. ERA is a parametric identification technique first introduced by Juang [8]. ERA produces a significant reduction in computation cost and memory resources. This method was first used in fluid mechanics in [9] and [10] for system identification purposes, whereas [11] used it to find an exploitable reduced order model for the synthesis of an efficient controller for noise reduction in a cavity flow.

Applying ERA on unstable systems generally requires prior knowledge of a controller which maintains the system in the vicinity of the unstable equilibrium point. Then, ERA is used in closed-loop configuration to extract the unstable dynamics [12, 13]. [11] used this method to identify the model of a compressible flow past a cavity, after the unstable equilibrium point be stabilized by using a dynamic phasor model, as in [14].

The usual description of the mechanism for cavity oscillations involves self-sustained oscillations, caused by the familiar Rossiter mechanism as described in [15]. The model consists of separate blocks of transfer functions. Each block represents a physical phenomenon. Their identification could be achieved in a closed-loop configuration from spectral analysis [16]. However, in the presence of noise, the spectral analysis promotes a biased model, due to the ignored correlation between the system input and the noise measurement [17, 18]. Therfore, we rule out this procedure of identification.

We here plan to apply the same procedure as [11] in order to identify a model that describes the linear instability of the steady base flow of an open cavity flow, in the incompressible regime. The instability eventually saturates into a limit cycle, which corresponds to the strong self-sustained oscillations experimented by the shear-layer. As reported in [14], the key point here is to be able to first suppress the limit cycle with a suitable non-linear controller. We do so by using an original time-delayed feedback controller, which eventually reveal to be robust against variations of the Reynolds number and geometry configuration.

The outline of the paper is as follows. In section 2 we introduce the technique ERA for closed-loop identification. In section 3 we detail the cavity flow configuration and the way the actuator is numerically implemented. The time-delayed feedback control used to stabilise the unstable equilibrium point is described in section 4. In section 5 we present the H_2-synthesis. Finally, in section 6, some numerical results are presented to illustrate the pertinence of ERA to identify an appropriate linear model for an optimal controller synthesis.

2. EIGENSYSTEM REALIZATION ALGORITHM FOR CLOSED-LOOP IDENTIFICATION

ERA was introduced in [8] to compute a state-space model from input and output data of stable systems. This technique is based on impulse response histories that are known as Markov parameters. It is generally not possible to directly identify an unstable system from an open-loop configuration. For unstable systems, the identification is only possible in closed-loop configuration, namely an unstable system made stable by dynamic feedback control. Then, an input excitation with large band-width is added in closed-loop operation such that it does not affect the overall system stability. Authors in [12] extends the ERA identification method to closed-loop system identification, in the so-called Observer/Controller Identification (OCID). This technique assumes the controller dynamics to be unknown and the controller be a full-state feedback, based on an observer, as shown in Figure 1. For closed-loop system identification with a known dynamics controller, see [13].

Consider a discrete linear system described by the state space model:

$$\begin{cases} x(k+1) = Ax(k) + Bu(k), \\ \quad y(\mathrm{k}) = \mathrm{C}\,x(k) + Du(k), \end{cases} \tag{1}$$

where $x \in \mathbb{R}^n$, $u \in \mathbb{R}^j$, and $y \in \mathbb{R}^q$. A, B, C and D are respectively state, input, output and feedthrough matrices. The input $u(k)$ of the system is the sum of the estimated vector state $\hat{x}(k)$ weighted by L and the broadband excitation $e(k)$:

$$u(k) = L\,\hat{x}(k) + e(k) = u_f(k) + e(k). \tag{2}$$

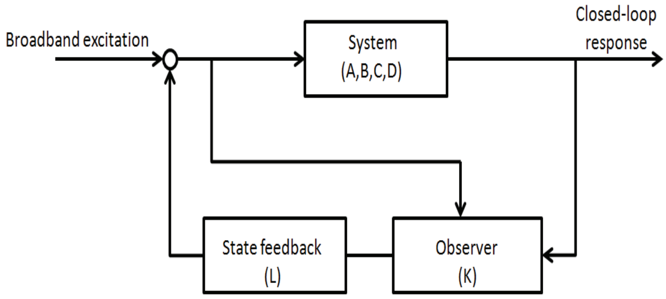

Figure 1. Schematic description of the identification of system when operating in closed-loop.

Estimation of the discrete state vector is provided by an observer with gain K:

$$\begin{cases} \hat{x}(k+1) = A\hat{x}(k) + Bu(k) - K\left[y(\mathrm{k}) - \hat{y}(\mathrm{k})\right], \\ \hat{y}(\mathrm{k}) = C\hat{x}(k) + Du(k), \end{cases} \tag{3}$$

which yields the system input-ouput relation in the form of the observer/controller system given as:

$$\begin{cases} \hat{x}(k+1) = \bar{A}\hat{x}(k) + \bar{B}\begin{bmatrix} u(k) \\ y(k) \end{bmatrix}, \\ \begin{bmatrix} \hat{y}(k) \\ u_f(k) \end{bmatrix} = \bar{C}\hat{x}(k) + \bar{D}u(k), \end{cases} \tag{4}$$

where

$$\bar{A} = A + KC, \qquad \bar{B} = \left[B + KD - K\right],$$
$$\bar{C} = \begin{bmatrix} C \\ -L \end{bmatrix}, \qquad \bar{D} = \begin{bmatrix} D \\ 0 \end{bmatrix},$$

The relationship between the input-ouput of the observer/controller system can be written in terms of a finite number of Markov parameters $\bar{Y}(i)$, provided that the observer:

$$\begin{bmatrix} \hat{y}(k) \\ u_f(k) \end{bmatrix} = \sum_{i=1}^{l} \bar{Y}(i)v(k-i) + \bar{D}u(k) \tag{5}$$

is stable. Indeed, (5), with:

$$v(k) = \begin{bmatrix} u(k) \\ y(k) \end{bmatrix}, \qquad \bar{Y}(0) = \bar{D},$$

$$\bar{Y}(k) = \begin{cases} \bar{C}\,\bar{A}^{k-1}\,\bar{B} & \text{if } k = 1, 2, \dots, l \\ 0 & \text{if } k \geq l \end{cases}$$

where l is large enough so that the observer converge. Convergence means that the estimated variables tend to the exact values. Indeed in that case the error between $x(t)$ and $\hat{x}(t)$ tends to zero when the number l is large. Thus the estimated output $\hat{y}(k)$ and the estimated state $\hat{x}(k)$ can be replaced by $y(k)$ and $x(k)$ into equation (4), respectively beyond l time steps. Consequently, equation (5) can be expressed in matrix form as:

$$y_t = \bar{Y}V, \tag{6}$$

for a length $N \gg l$ of available data, where

$$y_t = \begin{bmatrix} y(l) & y(l+1) & \dots & y(N) \\ u_f(l) & u_f(l+1) & \dots & u_f(N) \end{bmatrix},$$

$$\bar{Y} = \begin{bmatrix} \bar{D} & \bar{C}\bar{B} & \dots & \bar{C}\bar{A}^{l-1}\bar{B} \end{bmatrix},$$

$$V = \begin{bmatrix} u(l) & u(l+1) & \dots & u(N) \\ v(l-1) & v(l) & \dots & v(N-l) \\ \vdots & \vdots & \ddots & \vdots \\ v(0) & v(1) & \cdots & v(N\text{-}l) \end{bmatrix}.$$

The additive excitation e must be taken sufficiently rich such that V be full rank in order to identify the Markov parameters of the observer/controller system from equation (6), as:

$$\bar{Y} = y_t V^{+}, \tag{7}$$

where V^{+} denotes the pseudo-inverse of matrix V.

Now, we show how to separately compute the Markov parameters of the observer, system and controller gain, which are necessary to construct the Hankel Matrix. From the Markov parameters, we identify the constituent matrices of the state space representation of the unstable system. Sarting from equation (7), the Markov parameters of the observer/controller system can be identified at each time steps as:

$$\begin{aligned} \bar{Y}(0) &= \begin{bmatrix} D \\ 0 \end{bmatrix} = \begin{bmatrix} \bar{Y}^{(1,1)}(0) \\ \bar{Y}^{(2,1)}(0) \end{bmatrix}, \\ \bar{Y}(k) &= \begin{bmatrix} C \\ -L \end{bmatrix} (A+KC)^{k-1} \begin{bmatrix} B+KD & -K \end{bmatrix}, \\ &\equiv \begin{bmatrix} \bar{Y}^{(1,1)}(k) & -\bar{Y}^{(1,2)}(k) \\ -\bar{Y}^{(2,1)}(k) & \bar{Y}^{(2,2)}(k) \end{bmatrix}, \quad k = 1, 2, \cdots, l. \end{aligned} \tag{8}$$

From these identified Markov parameters, we easily deduce the individual Markov parameters of the observer, the system and the controller gain, which are put in the form:

$$\begin{aligned} Y^{(1,1)}(0) &= D, \\ Y(k) &= \begin{bmatrix} C \\ L \end{bmatrix} A^{k-1} [B \quad K] = \begin{bmatrix} CA^{k-1}B & CA^{k-1}K \\ LA^{k-1}B & LA^{k-1}K \end{bmatrix}, \\ &\equiv \begin{bmatrix} Y^{(1,1)}(k) & Y^{(1,2)}(k) \\ Y^{(2,1)}(k) & Y^{(2,2)}(k) \end{bmatrix}, \quad k = 1, 2, \ldots, l. \end{aligned} \tag{9}$$

The Markov parameters of the system and the observer, $Y^{(1,1)}(k)$ and $Y^{(1,2)}(k)$, are obtained from $Y^{(1,1)}(k)$ and $Y^{(1,2)}(k)$, respectively, by solving the following equation system [12]:

$$\begin{aligned} Y^{(1,1)}(k) &= \bar{Y}^{(1,1)}(k) - \sum_{i=1}^{k} \bar{Y}^{(1,2)}(i) Y^{(1,1)}(k-i), \\ Y^{(1,2)}(k) &= \bar{Y}^{(1,2)}(k) - \sum_{i=1}^{k-1} \bar{Y}^{(1,2)}(i) Y^{(1,1)}(k-i). \end{aligned} \tag{10}$$

We can put these recursive equations in matrix form as:

$$\begin{bmatrix} I & & & & \\ \bar{Y}^{(1,2)}(1) & I & & & \\ \bar{Y}^{(1,2)}(2) & \bar{Y}^{(1,2)}(1) & I & & \\ \vdots & \vdots & \ddots & & \\ \bar{Y}^{(1,2)}(i-1) & \bar{Y}^{(1,2)}(i-2) & \cdots & \bar{Y}^{(1,2)}(1) & I \end{bmatrix} \cdot \begin{bmatrix} Y^{(1,1)}(0) \\ Y^{(1,1)}(1) \\ Y^{(1,1)}(2) \\ \vdots \\ Y^{(1,1)}(i) \end{bmatrix}, = \begin{bmatrix} \bar{Y}^{(1,1)}(0) \\ \bar{Y}^{(1,1)}(1) \\ \bar{Y}^{(1,1)}(2) \\ \vdots \\ \bar{Y}^{(1,1)}(i) \end{bmatrix}. \tag{11}$$

$$\begin{bmatrix} I & & & & \\ \bar{Y}^{(1,2)}(1) & I & & & \\ \bar{Y}^{(1,2)}(2) & \bar{Y}^{(1,2)}(1) & I & & \\ \vdots & \vdots & \ddots & & \\ \bar{Y}^{(1,2)}(i-1) & \bar{Y}^{(1,2)}(i-2) & \cdots & \bar{Y}^{(1,2)}(1) & I \end{bmatrix} \cdot \begin{bmatrix} Y^{(1,2)}(1) \\ Y^{(1,2)}(2) \\ Y^{(1,2)}(3) \\ \vdots \\ Y^{(1,2)}(i) \end{bmatrix}, \\ = \begin{bmatrix} \bar{Y}^{(1,2)}(1) \\ \bar{Y}^{(1,2)}(2) \\ \bar{Y}^{(1,2)}(3) \\ \vdots \\ \bar{Y}^{(1,2)}(i) \end{bmatrix}. \tag{12}$$

To reach a sufficiently long and rich excitation, it is necessary to choose l very large. Since most physical systems have noise and nonlinearity, l very large ensures the accuracy and uniqueness of the Markov parameters $Y^{(1,1)}$ and $Y^{(1,2)}$. l is chosen such that the product lq be greater than the state number n of system, where q is the dimension of y. The remaining Markov parameters $\bar{Y}^{2,1}(k)$ and $\bar{Y}^{2,2}(k)$ are recovered from the following equations, as described in [12]:

$$\begin{aligned} Y^{(2,1)}(k) &= \bar{Y}^{(2,1)}(k) - \sum_{i=1}^{k} \bar{Y}^{(2,2)}(i) Y^{(1,1)}(k-i), \\ Y^{(2,2)}(k) &= \bar{Y}^{(2,2)}(k) - \sum_{i=1}^{k=1} \bar{Y}^{(2,2)}(i) Y^{(1,2)}(k-i). \end{aligned} \tag{13}$$

The open-loop system is then obtained by applying a classical ERA for the open-loop identification upon the set of Markov parameters identified from equations (11)–(13). This is performed by primarily forming the Hankel matrix of $Y(k)$ as:

$$H(k-1) = \begin{bmatrix} Y(k) & Y(k+1) & \cdots & Y(k+\gamma-1) \\ Y(k+1) & Y(k+2) & \cdots & Y(k+\gamma) \\ \vdots & \vdots & \cdots & \vdots \\ Y(k+\beta-1) & Y(k+\beta) & \cdots & Y(k+\beta+\gamma-2) \end{bmatrix}, \tag{14}$$

where γ and β are intergers satistying $\gamma_j \gg n$ and $\beta q \gg n$. Then, we must perform a singular value decomposition of the Hankel Matrix $H(0)$ and keep the s most significant singular values:

$$H(0) = R\Sigma Q^T \cong R_S \Sigma_S Q_S^T, \tag{15}$$

where s represents the reduced order of the system. For more details on how to extract the realisation of the open-loop system, see [8]. The identification of system matrices A, B, C, state feedback gain matrix L and observer gain K, is done as:

$$\begin{aligned} H(1) = R_S \textstyle\sum_S^{1/2} A \sum_S^{1/2} Q_S^T, \quad A = \sum_S^{-1/2} R_S^T H(1) Q \sum_S^{1/2}, \\ [B \quad K] = \textstyle\sum_S^{1/2} Q_S^T E, \\ \begin{bmatrix} C \\ L \end{bmatrix} = R^T R_S \textstyle\sum_S^{1/2}, \end{aligned} \tag{16}$$

where matrix E is constructed as follows:

$$E^T = \begin{bmatrix} I_h & O_h & \cdots & O_h \end{bmatrix}, \qquad h = j+q, \tag{17}$$

where m is the dimension of u.

3. CONFIGURATION AND BASIC FLOW PROPERTIES

3.1. Cavity Flow

Cavity flows are primarily characterized by their impinging shear-layer, which is known to be unstable against Kelvin-Helmholtz modes. The vortices generated by this instability are eventually advected downstream of the shear-layer, until they reach the cavity trailing edge, causing a pressure perturbation which is instantaneously fed back to the cavity leading edge, in the incompressible regime. The feedback reinforce the shear-layer instability, until a limit cycle is reached in which the shear-layer oscillations are self-sustained and strongly energetic at very well-defined frequencies in the spectrum. Additionally, a second loop take place through the inside cavity flow recirculation. This mechanism is sketched in Figure 2.

The frequencies of the self-sustained oscillations can be discriminated by performing a simple spectral analysis of the velocity or the pressure at the downstream impinging corner of the cavity. Moreover, they can be predicted using the empirical Rossiter formula [19]:

$$\frac{f_m L}{u_\infty} = \frac{m-\alpha}{Ma + \dfrac{1}{\kappa}}, \qquad m = 1, 2, 3, \cdots \tag{18}$$

at Mach number Ma $\to 0$, with $\kappa = c_p/u_\infty$, where c_p is the mean phase speed. In (18), f_m is the frequency at a given mode number m. The corrective coefficient α is used to model the phase shift in the loop.

The study is carried out in direct numerical simulations of a two-dimensional incompressible flow over a rectangular cavity. We are dealing with a shallow cavity of aspect ratio $L/D = 2$, where $L = 0.1$ m and D are the cavity length and depth, respectively. A cartesian coordinate system (x, y), for streamwise and crosswise directions, respectively, is set midspan at the top of the upstream cavity wall. The total domain is meshed on 296×128 nodes, among which 96×64 are devoted to the cavity. The mesh is particularly refined close to the walls and at the cavity-top in order to enhance the spatial resolution of boundary layers and shear-layer. Usual non-sliding conditions are applied at the walls. The inlet flow is determined by Dirichlet boundary conditions. In order to limit the numerical domain size, and therefore CPU time-consumption, the upstream vein length has been reduced. The inlet velocity profile is preliminary calculated by means of a 2D simulation of a laminar channel flow in spatial development, representative of the experimental upstream vein. The profile is then extracted out of the appropriate cross-section of the channel-flow and extruded in the spanwise direction. The laminar boundary layer at the cavity entrance is then developed from a leading edge set at a distance $L_l = 0.25$ m upstream of the cavity. The Reynolds number $\mathrm{Re} = u_\infty L/\nu$ is based on the cavity length L and the uniform flow rate velocity $u_\infty = 1.2$ m/s. The kinematic air viscosity $\nu = 16 \times 10^{-6}$ m^2/s. The momentum thickness of the laminar boundary layer upstream of the cavity is $\theta = 12.1 \times 10^{-4}$ m. In this configuration, the cavity oscillates at a single dominant frequency $f_2 = 13.0$ Hz, and harmonics, corresponding to the Strouhal number $\mathrm{St} = f_2 L/u_\infty \simeq 1$ (cavity mode $m = 2$ in equation (18)).

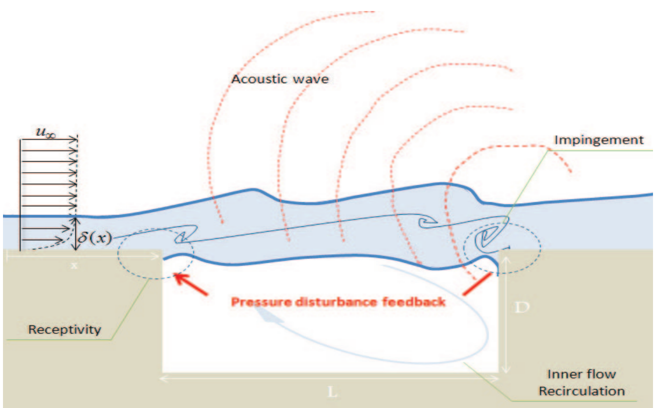

Figure 2. Schematic description of an open cavity flow.

The incompressible and isothermal flow dynamics is governed by the non-dimensional Navier-Stokes equations:

$$\begin{cases} \dfrac{\partial U}{\partial t} + (U \cdot \nabla)U = -\nabla P + \dfrac{1}{Re}\Delta U \\ \nabla \cdot U = 0 \end{cases} \tag{19}$$

where U is the velocity field and P the pressure field. Numerical simulations are performed with the OLORIN code developed at LIMSI, which is based on an incremental prediction projection method, see [20, 21] for more details. Momentum equations are discretised with a finite volume approach on a staggered structured grid. The spatial discretisation of fluxes is carried out with a second-order centred scheme in a conservative form and time derivation is approximated by a second-order backward differentiation formula. Viscous terms are implicitly evaluated whereas convective fluxes are explicitly estimated at time t^{+1} by means of a linear Adams-Bashford extrapolation. The discretised form of the Navier-Stokes equations yields a Helmholtz-type problem of the form:

$$\begin{cases} \left(I - \dfrac{2\Delta t}{3Re}\nabla^2 \right)(U^{\varsigma+1} - U^n) = -\nabla P^{\varsigma+1} + S^{\varsigma,\varsigma-1} \\ \nabla \cdot U^{n+1} = 0 \end{cases}$$

where superscript ς tags time t_ς, Δt is the time step and $S^{\varsigma,\varsigma-1}$ is the source term gathering all explicit quantities, evaluated at times t_ς and $t_{\varsigma-1}$. For each time-step, the numerical procedure is splitted in two parts, a prediction step and a projection step. The former consists in resolving the Helmholtz equation by considering the explicit pressure field P^ς in place of the implicit one. The integration is performed with an ADI (Alternating Direction Implicit) method [22]. As a result, we obtain an estimated velocity field U^* that is not yet divergence-free. The incompressibility property is imposed by using an incremental projection method [23]. The projection step requires to resolve a Poisson-type equation, using a relaxed Gauss-Seidel method coupled to a multigrid method, in order to accelerate convergence, where the source term relies on non-zero divergence of the predicted velocity field:

$$\nabla^2 \varphi = \rho_0 \nabla \cdot U^* / (2/3\Delta t).$$

Solution φ corresponds to the pressure time-increment, gradient $\nabla\varphi$ is the correction term such that the velocity field is divergence free at time $t^{\varsigma+1}$. The Poisson equation is commonly solved with Neumann-type boundary conditions, where the normal derivative on the domain limits is zero. By doing so, the boundary condition, on the corresponding normal velocity component, is not affected by the correction term.

3.2. Actuation Implementation

In order to manipulate the cavity flow, we introduce a bulk force $\vec{f}$ in the Navier-Stokes equations:

$$\rho\left(\frac{\partial \vec{u}}{\partial t} + (\vec{u}\,.\nabla)\vec{u} \right) = -\nabla p + \vec{f} + \mu\Delta\vec{u}, \tag{20}$$

which models the actuator. It is designed as an horizontal force in a small square area at the upstream edge of the cavity. This force is interpreted as an acceleration given to the fluid particles in this area. This way to model the actuator enables to inject a zero-net-mass flux but it brings a momentum (synthetic jet effect).

The pressure sensor located near the downstream edge is used in the feedback control configuration. Since the cavity has an unstable equilibrium point, it has first to be stabilized. This goal was achieved with a time-delayed feedback controller. The ERA technique described in section 2 with an unknown dynamics controller is then used for the identification of the system operating in close-loop (Figure 3). To successfully carry out the identification of a stabilized nonlinear system around an operating point, it is necessary to satisfy the superposition principle for an additive excitation. It guarantees that the system responds linearly at the operating point [16].

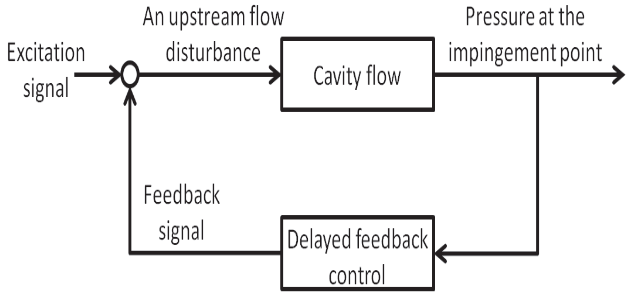

Figure 3. Identification of a reduced order model of the flow cavity.

4. DELAYED FEEDBACK CONTROL

The control strategy in phase opposition appears as a natural way to control an oscillatory system. Pressure fields are in phase (modulo 2π) at the upstream and downstream edges. However, a disturbance at the upstream edge needs time to travel down to the trailing edge. We propose to design the control law based on the delayed pressure measurement at the trailing edge, weighted by a gain a. Since there is no direct meaning of the phase response for nonlinear system, the delay and the gain are found by trial until the oscillations be killed. The control law is given as:

$$\vec{f} = \begin{bmatrix} f_x \\ f_y \end{bmatrix} \equiv \begin{bmatrix} ap(t-\tau) \\ 0 \end{bmatrix}, \tag{21}$$

where f_x and f_y are the x and y force components in the (xy) plane, respectively. The gain $a > 0$ determines the intensity of the applied force, and must be carefully chosen for not bringing the cavity into another undesired flow regime. Pressure p is measured at the downstream edge, and τ is the time

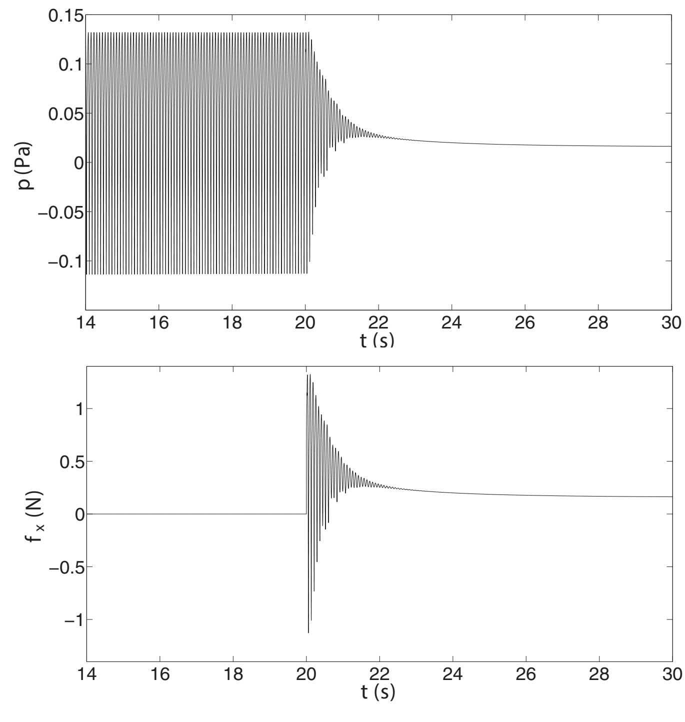

Figure 4. Closed-loop control with $f_x = a\, p(t - \tau)$ at Re = 7 500 with $\theta = 12.1 \times 10^{-4}$ m. The pressure at the impingement point (top) with the control input (bottom).

delay estimated from the dominant frequency $f_2 = 1/T_2$ of the oscillation of the shear layer. The optimal trial value of τ that kills the limit cycle is $\tau = T_2/6$, with a gain $a = 10$. Figure 4 illustrates the effectiveness of the control law. Control is switched on at $t = 20$ s, when the cavity is in its established regime (limit cycle). However, when the parameters of the control law are not optimal (in gain a or delay τ), the cavity switches to an other instability mode.

We next kept a and τ fixed and changed the Reynolds number from 7500 to 7000 and 8000. We observe that the command is robust to such changes in Re, although the frequency of oscillations slightly changes from 13 Hz to 12 and 14 Hz, respectively, as can be seen in Figure 5. In all three spectrograms, the sensor signal exhibits no more energy at the shear-layer frequency once the control has been turned on ($t = 20$ s). Unfortunately, we note that the control force applied to maintain the base flow stable is not vanishing, as shown in Figure 4. Henceforth, we slightly modified the control law in order to remove the asymptotic pressure. This is done by removing at any time the (slowly varying) mean pressure $p_{avg}(t)$, as:

$$f_x = a\,(p(t-\tau) - p_{avg}). \tag{22}$$

The mean pressure p_{avg} is calculated by a moving average filter with a window length T_{mean}. To get

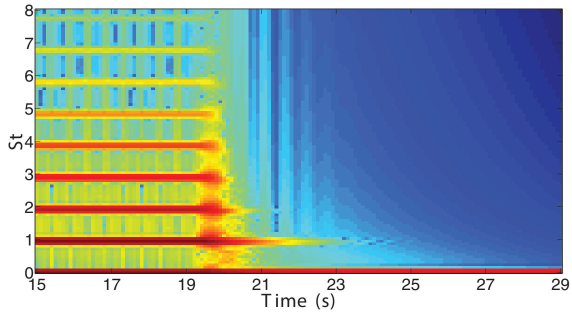

(a)

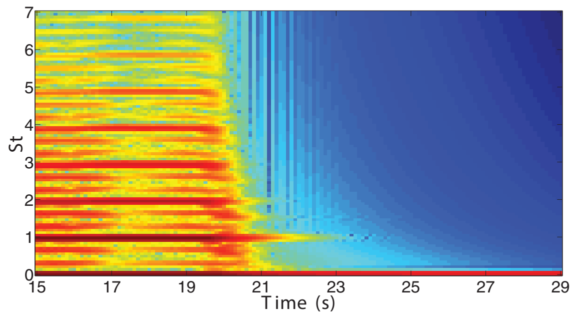

(b)

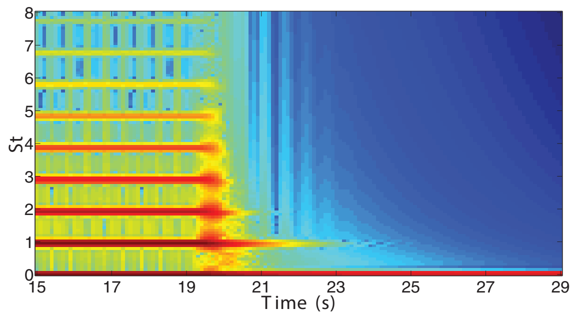

(c)

Figure 5. Performance of the closed-loop control with $f_x = a\,p(t-\tau)$ for various cavity configurations. Spectrogram of pressure at the impingement point of the cavity at Re = 7000 with $\theta = 12.5 \times 10^{-4}$ m (a), (b) Re = 8000 with $\theta = 11.7 \times 10^{-4}$ m and (c) Re = 7500 with $\theta = 11.9 \times 10^{-4}$ m.

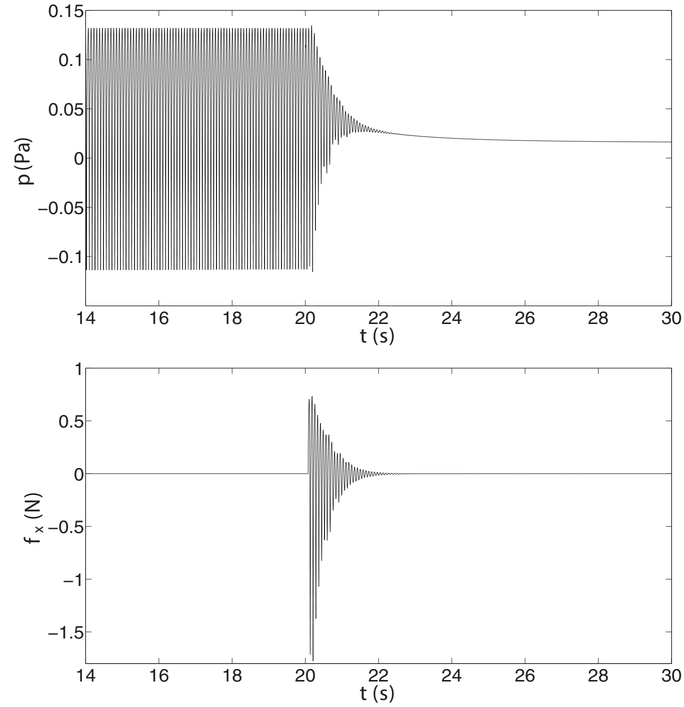

Figure 6. Closed-loop control with $f_x = a[p(t-\tau) - p_{avg}]$ of cavity at Re = 7500 with $\theta = 12.1 \times 10^{-4}$ m. The pressure at the impingement point (top) with the control input (bottom).

a satisfactory estimation of the mean pressure, we choose $T_{\text{mean}} = T_2$. There again, the oscillations are killed, but the command is now vanishing after a transient, as shown in Figure 6.

It is worth noticing that a time-delayed command is easy to implement experimentally. However, it does not provide any knowledge about the instability of flow. To fulfill this goal, we perform a parametric OCID identification that allows to shed light on the dynamics close to the vicinity of the unstable steady state. Even though the cavity dynamics experiment delays due to the convection of perturbations, OCID is able to approximate delays by the addition of poles and zeros in the model. This observation was made in [16] who emphasized that two additional states in the model were most probably due to the hydrodynamical delays in the cavity.

5. CONTROLLER DESIGN

In this section, we describe the H_2-synthesis of a controller from the reduced-order model of the flow cavity identified by using OCID. OCID provides a discrete-time model for the system, but for numerical convenience and better synthesis as we will see in the following we must convert the discrete-time model into a continuous-time model. We used the *d2c* command in Matlab (bilinear approximation of the derivative) for our continuous H_2-synthesis.

Let us consider the open-loop generalized plant G given in state-space representation as:

$$
\begin{aligned}
\dot{x} &= Ax + B_1 w + B_2 u, \\
z &= C_1 x + D_{11} w + D_{12} u, \\
y &= C_2 x + D_{21} w + D_{22} u,
\end{aligned}
\tag{23}
$$

with an exogenous input w representing external disturbances that modelizes as a unitary white-noise with a Gaussian distribution, an exogenous output z for performances specification, a control input u and a measurement ouput y.

The performance objective of the H_2-synthesis is to find a proper controller K given as:

$$
\begin{aligned}
\dot{x}_c &= A_c x_c + B_c y, \\
u &= C_c x_c .
\end{aligned}
\tag{24}
$$

which stabilizes G internally and minimize the H_2-norm of the transfer T_{zw} from w to z [24].

To find this proper controller and obtain a finite H_2-norm for the transfer function, the direct feedthrough from w to z is assumed to be zero $(D_{11} = 0)$ and we deal with systems having zero gain at infinite frequency ($D_{22} = 0$). Additional assumptions are made for the ouput feedback H_2-problem:

- (A, B_2, C_2) must be stabilizable and detectable.
- D_{12} must have full column rank and D_{21} must have full row rank.

Under these assumptions, the H_2-problem admits an H_2 optimal controller with A_c, B_c and C_c given as:

$$\begin{aligned} A_c &= A - B_2 B_2^T P_1 - Q_1 C_2^T C_2, \\ B_c &= Q_1 C^T, \\ C_c &= -B_2^T P_1, \end{aligned} \tag{25}$$

where the stabilizing matrices P_1 and Q_1 are solutions of the following algebraic Riccati equations:

$$\begin{aligned} A^T P_1 + P_1 A - P_1 B_2 B_2^T P_1 - C_1^T C_1 &= 0, \\ A Q_1 + Q_1 A^T - Q_1 C_1^T C_1 Q_1 + B_1 B_1^T &= 0, \end{aligned} \tag{26}$$

The above assumptions can be relaxed by using an optimization problem under Linear Matrix Inequalities (LMI).

We conducted this synthesis on the reduced-order models obtained with OCID for various cavity configuration. The resulting models have a direct feedthrough matrix D (Figure 7) which requires to undertake some arrangements in order to make the H_2-synthesis possible [24]. Figure 7 shows the controller design which stabilizes the cavity base flow, where w_1 and w_2 represent the state and measurement noise, respectively. In this case, the performance signal z contains the control signal f_x and the pressure measurement p at the impingement point, without measurement noise w_2. The exogenous input w contains w_1 and w_2. The open-loop generalized plant G thus becomes:

$$\begin{aligned} \dot{x} &= [A]x + [0 \quad B]w + [B]f_x, \\ \underbrace{\begin{pmatrix} f_x \\ \hat{p} \end{pmatrix}}_{z} &= \begin{bmatrix} 0 \\ C \end{bmatrix} x + \begin{bmatrix} 0 & 0 \\ 0 & D \end{bmatrix} \underbrace{\begin{pmatrix} w_2 \\ w_1 \end{pmatrix}}_{w} + \begin{bmatrix} 1 \\ D \end{bmatrix} f_x, \\ p &= [C]x + [1 \quad D]w + [D]f_x. \end{aligned} \tag{27}$$

We note that $D_{11} \neq 0$ and $D_{22} \neq 0$, hence the H_2 optimal controller can not be obtained. To find such an H_2 optimal controller, we first consider $D_{22} = 0$ and resolve the H_2 control problem with direct disturbance feedforward [24].

The first step is to find a compensator $\hat{K}$ with a standard H_2 synthesis (see above) from a model of transition $\hat{G}$ given in matrix form as:

$$\hat{G} = \left[\begin{array}{c|cc} A + B_2 D_k C_2 & B_1 + B_2 D_k D_{21} & B_2 \\ \hline C_1 + D_{12} D_k C_2 & 0 & D_{12} \\ C_2 & D_{21} & 0 \end{array} \right], \tag{28}$$

with

$$D_k = -D_{12}^T D_{11} D_{21}^T.$$

where B_1, C_1, D_{11}, D_{12} and D_{21} are those of equation (27) times ponderation matrices to take into account the noise power model. Then the corrector K_{GD} for G with $D_{22} = 0$ is given by:

$$K_{GD} = D_k + \hat{K}. \tag{29}$$

In the second step, $D_{22} = 0$, the controller is deduced from equation (29) as:

$$K_G = K_{GD}(1 - D_{22} K_{GD})^{-1}. \tag{30}$$

This linear controller aims to validate the model that captures the linear dynamics of the cavity,

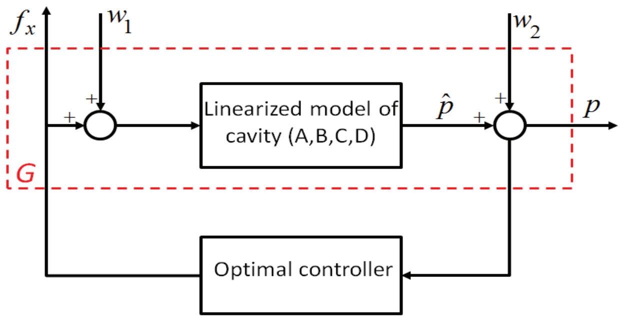

Figure 7. Standard feedback configuration for the H_2 controller synthesis.

identified by OCID. This approach, where a linear controller developed from the linearized dynamics of a nonlinear system stabilizes the complete system, was already seen in [25] and [11] for the stabilization of combustion oscillations as well as, the cavity oscillations of a compressible flow [16], where a LQG compensator was synthesized.

6. SIMULATION RESULTS

We carried out the identification by OCID on various cavity configurations, changing both the Reynolds number and the momentum thickness θ. The models are validated by comparing the error between the impulse response of the reduced model and that provided by the Markov parameters. Figure 8 shows the frequency response of the linearized model for a 23-dimensional state in the flow cavity at Re = 7500 and momentum thickness $\theta = 12.1 \times 10^{-4}$ m. The synthesized controllers (see section 5) suppress the oscillations of the cavity flow. Thus, the validity of the identified model is confirmed, as illustrated in Figure 9, where the optimal control is switched on at t = 20 s. Because not all unstable dynamics are captured, we point out that performing a balanced truncation of smaller dimension does not allow to find any stabilizing corrector for this cavity configuration.

Models also teach us about the dynamics responsible for the appearance of oscillations in the shear layer. Figure 10 shows the eigenvalues (poles) of the linear dynamics identified for two flow configurations, namely $\theta = 12.1 \times 10^{-4}$ and 11.9×10^{-4} m at Re = 7500. In both cases, the most unstable mode in the model, at the utmost right of the imaginary axis, corresponds to the dominant frequency of the shear layer oscillations (St $\simeq$ 1). The least unstable mode, closest to the imaginary axis in the right-half plane, is associated with a Strouhal number of the order of 1.5. This value is typical of the shear-layer mode m = 3 in equation (18). It suggests that the linear model can actually detect Rossiter modes, though the flow usually never spontaneously oscillates at those frequencies. Yet, this mode is excited when a disturbance is applied in the boundary layer, at the cavity upstream edge, either in open-loop or closed-loop control, with a controller that does not stabilize this unstable

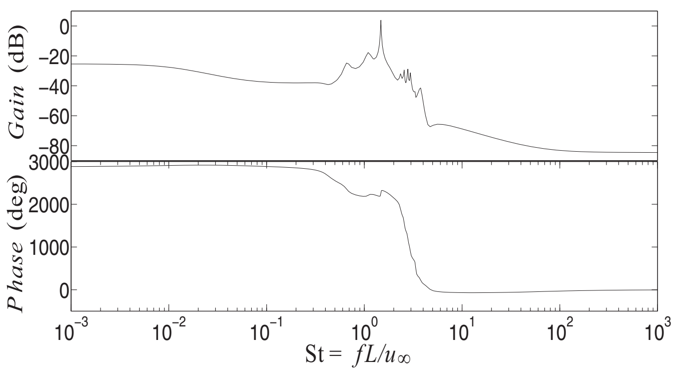

Figure 8. Magnitude and phase of frequency response of the 23-dimensional state linearized model of cavity at Re = 7500 with a momentum thickness $\theta = 12.1 \times 10^{-4}$ m.

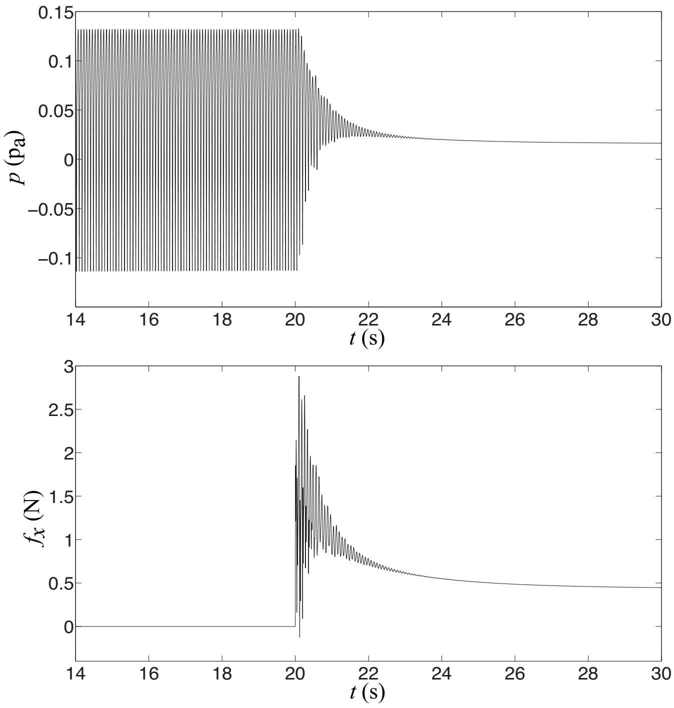

Figure 9. Closed-loop optimal control of cavity at Re = 7500 with a momentum thickness equal to 12.12 × 10^{-4} m. The pressure at the impingement point (top) with the control input (bottom).

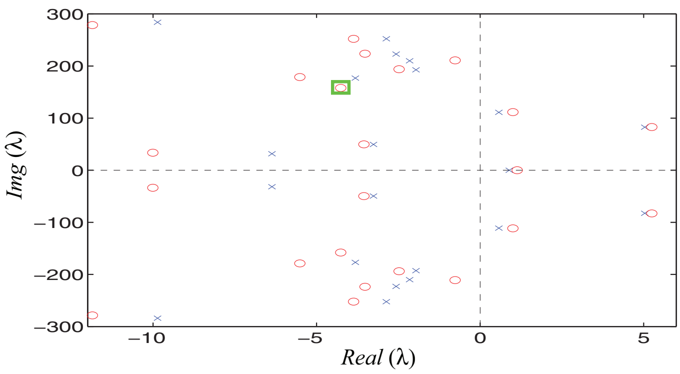

Figure 10. Comparison of the eigenvalues of the reduced order models of a flow cavity at Re = 7500 with two different momentum thicknesses: 12.12 × 10–4m (blue crosses) and 11.88 × 10–4 m (red circles).

mode. This is, for instance, what happens when the optimal controller synthesized for $\theta = 12.1 \times 10^{-4}$ m is applied to the cavity flow with momentum thickness $\theta = 11.9 \times 10^{-4}$ m, where the least unstable mode is not stabilized. For the cavity configuration $\theta = 11.7 \times 10^{-4}$ m at Re = 8000, the signature of the least unstable mode (see Figure 15) becomes noticeable in the cavity flow without control, as shown in Figure 5 (b). The signature of this mode is however not permanent in time: it suddenly occurs and is accompanied by other frequencies, which presumably result from nonlinear interactions between the unstable modes. This behavior is reminiscent of the *mode switching* phenomenon experimentally observed in incompressible [26, 27, 28] as well as compressible cavity flows [29].

When the momentum thickness of the laminar boundary layer upstream of the cavity is changed from $\theta = 12.1 \times 10^{-4}$ to 11.9×10^{-4} m, at Re = 7500, the shear layer oscillation frequency remains roughly unchanged, but its amplitude changes. We also note that a 25-dimensional state model is required to accurately describe the dynamics of the new cavity configuration. The change in momentum thickness actually gives rise to an additional stable mode for the dynamics, surrounded by a green box in Figure 10. We infer that this mode actually approximate the delay introduced by the advection of disturbances by the shear layer from the upstream to the downstream edges. Indeed, delays are often approximated by rational functions, whose accuracy increases with the polynomial order (Padé approximation). The additional mode could therefore be added to the model in order to better approximate the effect of the delay.

A real eigenvalue close to the imaginary axis was found for all linear models of investigated cavity configurations (see Figure 10 and 15). This eigenvalue likely models the action of the actuator on the flow. Indeed, the actuator is a bulk force, proportional to an acceleration, and therefore proportional to the time-derivative of the local velocity. The transfer function of a derivative plant provides a zero eigenvalue. Henceforward, it seems rather natural that such an eigenvalue occur in the model. However, this eigenvalue was found on the real axis. We assume that the shift of this eigenvalue with respect to the imaginary axis is due to the lack of precision of the linear model identified by balanced truncation.

The control signal f_x resulting from the optimal controllers are not vanishing, as shown in Figure 9. To get a vanishing command, we must subtract, here also, the mean pressure $p_{avg}(t)$ from p by using a moving average filter, as described in section 4. As the synthesized optimal controllers provide very low phase margin, we avoid to use high-pass filters to remove the nonzero mean pressure $p_{avg}(t)$ in order to not introduce a phase lag, which might destabilize the closed-loop system. As seen in Figure 11, the result is eventually very promising, since the control signal is of low intensity. Most noticeably, the (linear) optimal controller synthesized for Re = 7500 with $\theta = 11.9 \times 10^{-4}$ m, also stabilizes the linear models at Re = 7500, $\theta = 12.1 \times 10^{-4}$ m and at Re = 7000, $\theta = 12.5 \times 10^{-4}$ m, inferring a relative robustness of the controller. However, this controller could not stabilize the linear model at Re = 8 000, $\theta = 11.7 \times 10^{-4}$ m. The same range of robustness is observed in direct numerical simulations of the cavity flow, where the linear controller identified for Re = 7500, $\theta = 11.9 \times 10^{-4}$m, is switched on at t = 20 s on the three other configurations (see Figure12). However, when we synthesize an H_2 optimal controller from the reduced order model of the cavity flow at Re = 8 000 ($\theta = 11.7 \times 10^{-4}$ m) and implement it in direct numerical simulations, this cavity is stabilized

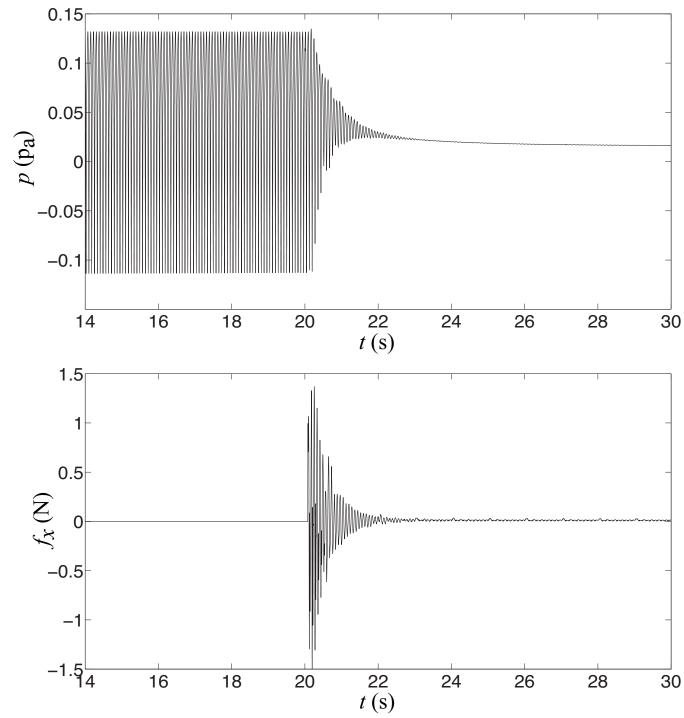

Figure 11. Closed-loop optimal control of a cavity at Re = 7500 with $\theta = 12.1 \times 10^{-4}$ m by a pressure feedback without its moving average $p_{avg}(t)$. The pressure at the impingement point (top) with the control input (bottom).

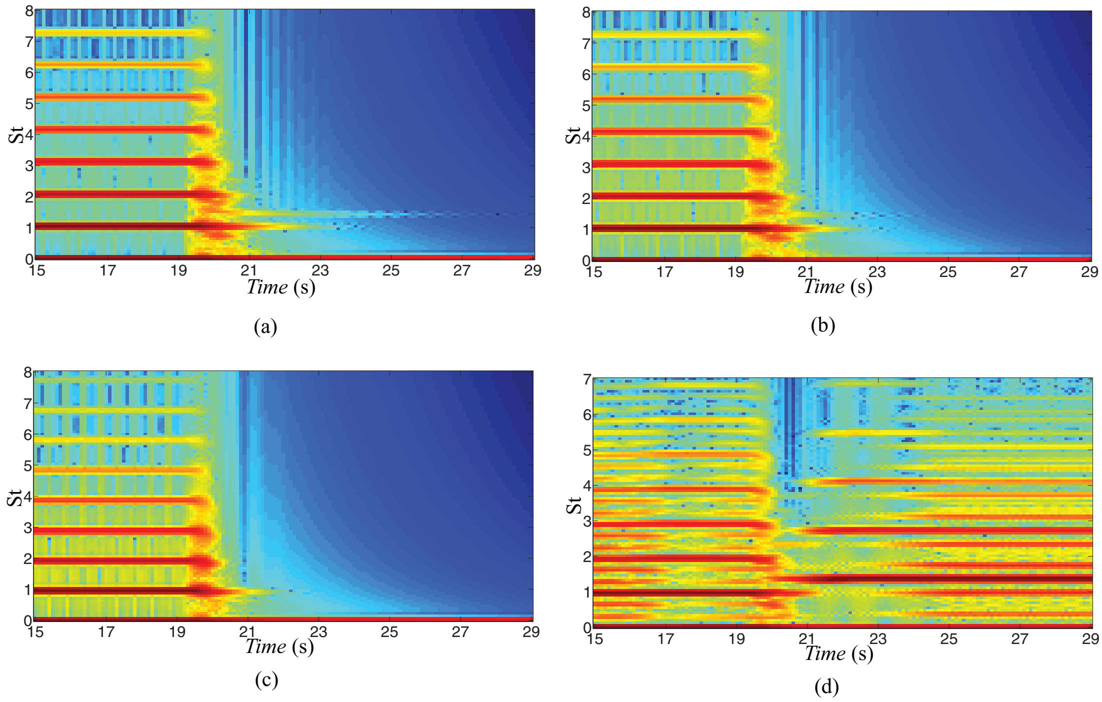

Figure 12. Performance of closed-loop control for various cavity configuration with the synthetized H2 optimal controller from the reduced order model for cavity at Re = 7500 with $\theta = 11.9 \times 10^{-4}$ m, showed from the spectrogram of the impingement pressure of the concerned cavity (a), (b), (c) and (d) for the flow cavity at Re = 7500 with $\theta = 12.1 \times 10^{-4}$ m, Re = 7000 with $\theta = 12.5 \times 10^{-4}$ m, and Re = 8000 with $\theta = 11.7 \times 10^{-4}$ m, respectively.

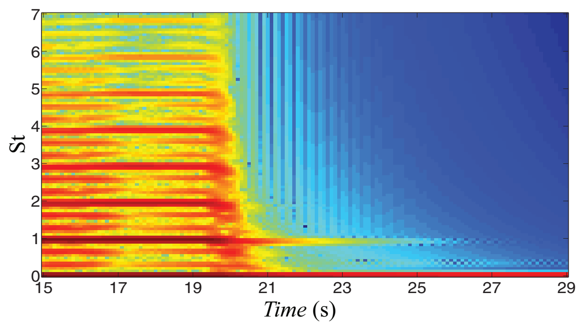

Figure 13. Performance of the synthetized H2 optimal controller for a cavity flow at Re = 8000 ($\theta = 11.7 \times 10^{-4}$ m).

(see Figure 13).

Although the delay controller described in Sec. 4 is able to stabilize the cavity steady base-flow in all the configurations investigated in this paper, it fails to stabilize the linear models. This suggests that the linear models identified by OCID are not fully accurate and that the delay controller does not stabilize all the unstable modes of the linear models. As can be seen in Figure 14, the unstable eigenvalue at low frequency in the closed-loop system, for Re = 7500 and $\theta = 12.1 \times 10^{-4}$ m, is not stabilized by the time-delayed feedback control. The reason is probably partly due to the truncation of equation (15), where the less energetic singular values are neglected. Those neglected singular values may actually corrupt the static gain identification. In addition, the nonlinear nature of the system may also contribute to the lack of precision in the identification. Yet, these linear models are useful to identify the most dominant dynamics in the cavity flow.

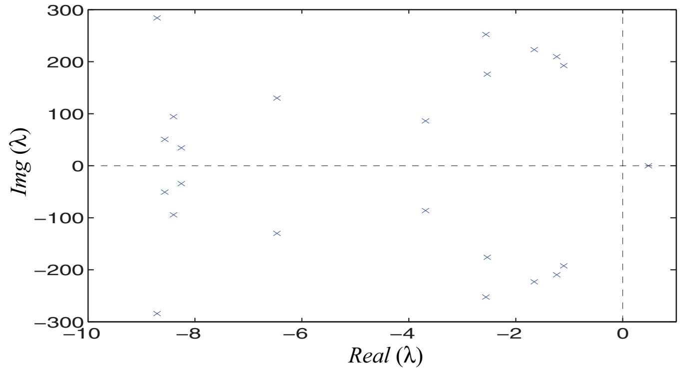

Figure 14. Closed loop eigenvalue of the reduced order models of a cavity flow at Re = 7500 (θ = 12.1 × 10^{-4}m) with the delayed feedback control.

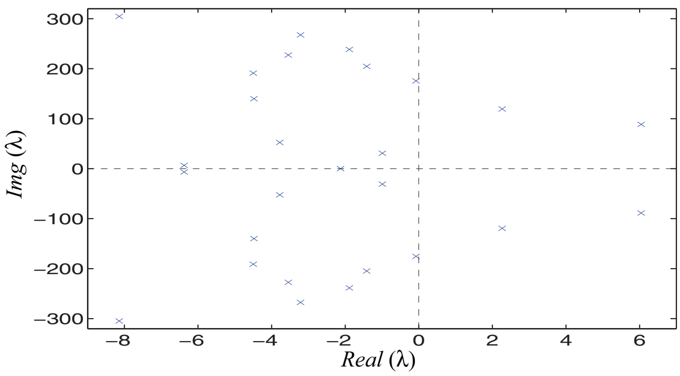

Figure 15. Eigenvalues of the reduced order models of a cavity flow at Re = 8000 and θ = 11.7 × 10^{-4}m.

CONCLUSION

In this paper, a method of robust nonlinear control to stabilize the cavity oscillations has been proposed. It is based on a time-delayed feedback control law, based on local pressure measurement. The delayed feedback controller reveals to be simple and robust to changes in cavity configuration (see Figure 4 and 5). This controller is also easy to implement experimentally without any prior knowledge of the cavity dynamics, but it does not allow to analyse the origin of the instability, and its consequences. However, thanks to this control, a closed-loop identification could be performed that identified a linearized model for the cavity. This identification method is based on balanced truncation (OCID). The linear dynamics are extracted from the Markov parameters of the closed-loop system in the form of a state space model. This model is of reduced-order and preserves both controllability and observability of the captured dynamics. A linear optimal control was synthesized from the linearized model of the cavity. This linear control shows some robustness to changes in cavity flow conditions.

REFERENCES

[1] Yoshida, T., Watanabe, T., Ikeda, T. and Iio, S., Numerical analysis of control of flow oscillations in open cavity using moving bottom wall, *JSME International Journal Series B,* 2005, 49(4), 1098–1104.

[2] Kegerise, M.A., Cattafesta, L.N. and Ha, C., Adaptive identification and control of flow induced cavity oscillations, *1st AIAA Flow Control Conference,* AIAA Paper, 2002, 3158.

[3] Rowley, C.W., Colonius, T. and Murray, R.M., Model reduction for compressible flow using pod and galerkin projection, *Physica D Nonlinear Phenomena,* 2004, 189(1–2), 115–129.

[4] Rowley, C.W., Model reduction for compressible flow using pod and galerkin projection, *International Journal of Bifurcation and Chaos,* 2005, 15(3), 997–1013.

[5] Barbagallo, A., SIPP, D. and Schmid, P.J., Closed-loop control of an open cavity flow using reduced-order models, *Journal of Fluid Mechanics,* 2009, 641, 1–50.

[6] Sipp, D. and Schmid, P., Closed-loop control of fluid flow: a review of linear approaches and tools for the stabilization of transitional flows, *Journal Aerospace Lab,* 2013, 6.

[7] Ahuja, S., Ph.D. thesis, *Reduction Methods for Feedback Stabilization of Fluid Flows,* Princeton University, 2009.

[8] Juang, J.N. and Pappa, R.S., An eigensystem realization algorithm for modal parameter identification and model reduction, *Journal of Guidance, Control, and Dynamics,* 1985, 8(5), 620–627.

[9] Cattafesta, L.N., Garg, S., Choudhari, M. and Li, F., Active control of flow-induced cavity resonance, *28th Fluid Dynamics Conference,* AIAA Paper, 1997, 1804.

[10] Cabell, R.H., Kegerise, M.A., Cox, D.E. and Gibbs, G.P., Experimental feedback control of flow-induced cavity tones, *AIAA,* 2006, 44(8), 1807–1815.

[11] Illingworth, S.J., Morgans, A.S. and Rowley, C.W., Feedback control of flow resonances using balanced reduced-order models, *Journal of Sound and Vibration,* 2011, 330(8), 1567–1581.

[12] Juang, J.N. and Phan, M., Identification of system, observer, and controller from closed-loop experimental data, *Journal ofGuidance, Control, and Dynamics,* 1994, 17(1), 91–96.

[13] Phan, M., Juang, J.N., Horta, L.G. and Longman, R.W., System identification from closed-loop data with known output feedback dynamics, *Journal of Guidance, Control, and Dynamics,* 1994, 17(4), 661–669.

[14] Rowley, C.W. and Juttijudata, V., Model-based control and estimation of cavity flow oscillations, *Proceedings of the 44th IEEE Conference on Decision and Control and European Control Conference,* Seville, Spain, 2005, 2, 512–517.

[15] Rowley, C.W., Williams, D.R., Colonius, T., Murray, R.M., G., M.D. and Fabris, D., Model-based control of cavity oscillations, part II: system identification and analysis, *40th AIAA Aerospace Sciences Meeting,* AIAA Paper, 2002, 0972.

[16] Illingworth, S.J., Morgans, A.S. and Rowley, C.W., Feedback control of cavity flow oscillations using simple linear models, *Journal of Fluid Mechanics,* 2012, 709, 223–248.

[17] Van Der Hopp, P., Closed-loop issues in system identification, *Annual reviews in control*, 1998, 22(7), 173–186.

[18] Forssell, U. and Ljung, L., Closed-loop identification revisited, *Automatica,* 1999, 35(7), 1215–1241.

[19] Heller, H.H., Holmes, D.G. and Covert, E.E., Flow induced pressure oscillations in shallow cavities. journal of Sound and vibration, *Journal of sound and Vibration,* 1971, 18(4), 545–553.

[20] Gadoin, E., Le Quéré, P. and Daube, O., A general methodology for investigating flow instabilities in complex geometries: application to natural convection in enclosures, *International Journal for Numerical Methods in Fluids,* 2001, 37(2), 175–208.

[21] Podvin, B., Fraigneau, Y., Lusseyran, F. and Gougat, P., A reconstruction method for the flow past an open cavity, *Journal of fluids engineering,* 2006, 128(3), 531–540.

[22] Hirsch, C., *Numerical computation of internal and external flows,* John Wiley and Sons, New York, USA, 1990.

[23] Guermond, J.L., Minev, P.D. and J., S., An overview of projection methods for incompressible flows, *Computer Methods in Applied Mechanics and Engineerings,* 2006, 195, 6011–6045.

[24] Zhou, K., Doyle, J. and Glover, K., *Robust and Optimal Control*, Prentice Hall, New Jersey, USA, 1996.

[25] Dowling, A.P. and Ffowcs Williams, J.E., *Sound and sources of sound,* Ellis Horwood, Chichester, UK, 1983.

[26] Basley, J., Pastur, L.R., Lusseyran, F., Faure, T.M. and Delprat, N., Experimental investigation of global structures in an incompressible cavity flow using time-resolved piv, *Experiments in Fluids,* 2011, 50(4), 905–918.

[27] Pastur, L.R., Lusseyran, F., Faure, T.M., Fraigneau, Y., Pethieu, R. and Debesse, P., Quantifying the non-linear mode competition in the flow over an open cavity at medium reynolds number, *International Journal of Aeroacoustics,* 2008, (4), 597–608.

[28] Lusseyran, F., Pastur, L. and Letellier, C., Dynamical analysis of an intermittency in an open cavity flow, *Physics of Fluids,* 2008, 20, 114–101.

[29] Garg, S. and Cattafesta III, L.N., Quantitative schlieren measurements of coherent structures in a cavity shear layer, *Experiments in Fluids,* 2001, 30, 123–134.